Malaysian Journal of Chemistry, 2025, Vol. 27(5), 190-199
(Special Issue: *5th IKMPB Online Symposium, IKMPB 2025*)

Effect of Gold Nanoparticle Size Conjugated with Graphene Quantum Dots on the Signal of a Fibre Optic Sensor

Nur Haziqah Izzati Roslan[1], Siti Rabizah Makhsin[1]*, Rozina Abdul Rani[1] and Beenish Siddique[2]
[1]Faculty of Mechanical Engineering, Universiti Teknologi MARA, 40450, Shah Alam, Selangor, Malaysia
[2]AEH Innovative Hydrogel Ltd, Graphene Engineering Innovation Centre, Sackville St, Manchester M1 3BB, United Kingdom
*Corresponding author (e-mail: sitirabizah@uitm.edu.my)

Graphene quantum dots (GQDs) and gold nanoparticles (AuNPs) are recognized as promising materials for sensing applications due to their exceptional photochemical properties. This study investigates the impact of AuNPs of sizes 30, 60, and 90 nm, when conjugated with blue-emission graphene quantum dots (b-GQDs), on the performance of a fibre optic sensor. The AuNPs were prepared using a seeding-growth method, while b-GQDs were synthesized through a microwave-assisted method. Characterization techniques, including UV-visible (UV-Vis) spectroscopy, fluorescence spectrophotometry, Zeta size analysis, and X-ray diffraction (XRD), were employed to confirm the optical properties, particle size, and crystallinity of the samples. Compared to the uncoated fibre optic probe, the 30 nm AuNPs coating alone enhanced the sensor signal by 42.5%, while the b-GQDs coating resulted in an 84.9% improvement. Remarkably, the hybrid structure of b-GQDs with 30 nm AuNPs achieved the highest signal enhancement of 143.5%, surpassing hybrids with larger AuNP sizes. These findings revealed a synergistic effect between b-GQDs and smaller-sized AuNPs, making it beneficial for the development of a highly sensitive fibre optic sensor.

Keywords: Blue graphene quantum dots; gold nanoparticles; fibre optic sensor; microwave; optical signal

Received: April 2025; Accepted: August 2025

The development of fibre-optic sensors has been further aided by the ability to generate high-quality optical fibres at low cost and in huge quantities [1]. Owing to its unique characteristics, such as its immunity to electromagnetic interference, biocompatibility, simple multiplexing capability, small size, and capacity to be used in extremely hazardous and corrosive environments, fibre optic sensors have gained popularity in many practical applications over the past ten years. The sensor can be used in a wide range of applications, such as structural health monitoring, medical and healthcare systems, semiconductor manufacturing, agriculture, food processing and storage, as well as many industrial processes. In these applications, the ability to precisely measure parameters such as temperature, strain, and relative humidity is crucial for maintaining safety, improving product quality, and increasing operational efficiency [2].

In upgrading the conventional fibre optic sensors, the sensing materials, such as those which are graphene-based [3], can be embedded into the sensor interface. The discovery of graphene has sparked considerable interest in graphene-based materials, particularly graphene quantum dots (GQDs), due to their attractive characteristics, including their convenience of synthesis and exceptional physical-chemical properties. GQDs exhibit the carbon structure of graphene. Carbon atoms are arranged in hexagonal rings, but with lateral dimensions of less than 100 nm. GQDs are regarded as 0D materials since they have less than ten atomic layers, and their dimensions are nanoscale. The bandgap that gives GQDs their luminous features is caused by quantum confinement and edge effects brought on by the alteration of the electron distribution, and it may be modified depending on the size and structure of the GQDs [4]. GQDs have a promising future in fields like fluorescent probes, optoelectronic devices, sensors, and cell imaging due to their significantly low toxicity, excellent solubility, high stability, stable photoluminescence, better surface grafting, high electrical conductivity, and high thermal conductivity [5].

Besides graphene-based materials, nanomaterials have also significantly reformed the landscape of conventional fibre optic sensors. The unique properties of nanomaterials combined with the advancement of fabrication techniques bring opportunities to achieve exceptional sensitivity and selectivity, along with integrated multifunctional interfaces, thereby enabling the development of versatile sensors [6]. The physical, material and chemical properties of nanomaterials strongly correlate with their inherent compositions, apparent sizes, and extrinsic surface structures. Gold

†Paper presented at the 5th IKMPB Online Symposium: Sustainable Chemistry Innovations Shaping the Future Life

nanoparticles (AuNPs), for instance, are well-suited to enhancing of the sensor performance due to their size-dependent physicochemical properties, high electrocatalytic activity, excellent chemical stability and functional compatibility with various molecules and polymers. These features enhance charge transfer kinetics and increase the effective surface area at the sensing interface, thus improving the sensitivity and responsiveness of the sensor [7].

In sensing mechanisms utilizing localized surface plasmon resonance (LSPR), at the metal–dielectric interface, AuNPs absorb part of the incident optical energy. This energy is converted into an electromagnetic wave, which manifests as a distinct absorption peak in the transmission spectrum at a specific wavelength. During the LSPR event, the conduction electrons in the AuNPs oscillate coherently in response to the electromagnetic field, whereby the size, shape and aggregation state of AuNPs will influence the position of the LSPR absorption band. For instance, the LSPR signals of AuNPs are often observed occurring at ~530 nm for a size of ~20 nm [8].

Fakhri et al. [9] reported that the sensitivity of a fibre optic sensor for detecting glycerol solution had been significantly enhanced, reaching a value of 3157.98 nm/RIU by depositing 50 nm of AuNPs onto the unclad silica core (single-mode) of the fibre. In this setup, light propagation within the fibre generated evanescent waves that interacted with the external surface, thus enabling the use of an unclad fibre to interact with the analyte presence for the detection to be measured. Moreover, Makhsin et al. [10] demonstrated that on the same single-mode fibre optic sensor, smaller AuNPs (4 nm) generated a stronger optical signal compared to larger particles, while integrating AuNPs with an agarose hydrogel matrix significantly enhanced the sensor's performance, achieving a glycerol solution RI sensitivity of 3669.8 ± 5.232 nm/RIU. This was evidence of the synergistic effect of AuNPs size and material hybridization in optimizing the signal output of the fibre optic sensor. Meanwhile, a rapid on-site detection of glucose was successfully fabricated using fibre optic-based material modified with annine functionalized GQDs embedded hydrogel film, which demonstrated a fast increase of fluorescence signal toward glucose with a response time of approximately 0.44 s [11].

Hence, more effort should be conducted to comprehend the advantages of signal amplification with rapid detection by integrating the AuNPs with GQDs. We reported the synthesis of hybrid nanostructures of AuNPs with blue emission of GQDs (b-GQDs) as sensing materials, with a modified fibre optic sensor configuration. 30, 60 and 90 nm sizes of AuNPs were synthesized using a seeding-growth method. For simplicity and cost efficiency, the microwave-assisted method was applied to synthesize GQDs. b-GQDs-AuNPs were deposited on the unclad fibre optic and function as a sensitive area in the sensor configuration. It is believed that the synergy between AuNPs and b-GQDs can elevate the optical properties, thus significantly enhancing the sensor signal.

METHODOLOGY

Materials and Chemicals

All the chemical reagents were analytical grade and were utilized without further purification. Citric acid (≥99.5%, Sigma-Adrich), sodium hydroxide; NaOH, (99%, Merck) and hydrochloric acid; HCl (≥37%, Merck) were used to synthesize b-GQDs. For AuNPs, hydroxylamine hydrochloride (99%, Sigma-Adrich), gold (III) chloride trihydrate (≥99.9%, Sigma-Aldrich), trisodium citrate (≥99%, Sigma-Aldrich) and sodium azide, NaN_3 (=99.5%, Sigma-Aldrich) were used. The buffer solution, phosphate buffer saline; PBS; (Sterile, pH 7.2), was purchased from Sigma-Adrich, while ultrapure deionized water (DI water, 18.2 MΩ·cm at 25 °C) was obtained from Millipore. Before synthesis, the glassware was cleaned using an aqua regia solution made of a 3:1 ratio of HCl to nitric acid; HNO_3 (65%, Merck). For Ethyl-3-(dimethyl aminopropyl) carbodiimide hydrochloride; EDC (≥98.0%, Sigma-Adrich) was used as a linker during conjugation of AuNPs to b-GQDs. 1 meter of single-mode silica core of fibre (SOF) optic patch cord with FC-FC pigtails (YP-Link, China) was used to prepare the sensor platform.

Synthesis of b-GQDs

b-GQDs were synthesized using the reduction of citric acid, using a microwave-assisted method. To begin with, 1.0 g of citric acid was heated in the microwave (Model SHARP, R207EK, 800W) for 20 minutes. Then, the melted citric acid was placed on the hotplate stirrer, and 100 mL of 0.25M NaOH solution was then gradually added to the solution with vigorous stirring at 600 rpm for 10 minutes. The pH of the solution obtained was measured at a pH of 13. The pH was adjusted to pH 8.0 by carefully dropping 5% v/v HCl solution in order to create an aqueous solution of GQDs that was luminescent blue under UV light. Table 1 shows the summary of the parameters involved in optimizing the synthesis of b-GQDs, with each sample ID named from A to G.

Table 1. Summary of synthesis parameters of b-GQDs samples.

Sample	Sample ID	Microwave time (mins)	Weight of citric acid (g)	NaOH
b-GQDs	**A**	20	2.0	0.25 M, 100 mL
	B	30		
	C	40		
	D	30	0.5	
	E		1.0	
	F		2.0	
	G		3.0	

Synthesis of AuNPs

The seed growth process was used to prepare AuNPs, slightly modified from a previously published method [12]. To start with, the glassware was cleaned using aqua regia solution (1:3 of HNO_3: HCl), then thoroughly rinsed to remove any residue. For the formation of AuNPs seeds, 125 mL of 254 M gold chloride solution ($HAuCl_4$) was poured into a 250 mL Erlenmeyer flask and the solution was heated to 300 °C with a stirring speed of 350 rpm. At the boiling condition, 2.5 mL of 40 mM trisodium citrate as a reducing agent was quickly added, and the boiling condition was maintained for another 10 minutes while being constantly stirred. The heat was then turned off, and the stirring was continued for another 15 minutes. Finally, the AuNPs seed solution was allowed to cool to room temperature.

At the growth stage, 10 mL of freshly produced seed solution was mixed with 50 mL of DI water to grow AuNPs to the sizes of 30 nm, 60 nm and 90 nm. After several minutes of stirring, 1 mL of freshly prepared 0.2 M hydroxylamine hydrochloride was added. The solution was then droplet-infused with 25.4 mM gold chloride (0.25, 1 or 3 mL) under the same stirring conditions as summarized in Table 2. The solution was continuously stirred for another 5 minutes to complete the reduction process. The experiment was conducted at room temperature with a stirring speed of 350 rpm, as hydroxylamine is a mild reducing agent which was able to reduce the Au at room temperature. To prevent contamination of the prepared AuNPs, 0.02 %w/v of sodium azide (*e.g.*, 0.01 g in a 50 mL solution of AuNPs) was added as a preservative to the solution. The AuNPs solutions were stored in the dark and refrigerated at 4 °C until they were used.

Synthesis of b-GQDs Conjugated with AuNPs (b-GQDs-AuNPs)

Conjugation of b-GQDs-AuNPs was performed by a method guided by [13]. Here, 0.038 g of EDC was dissolved in 1 mL of PBS buffer (pH 7.4) for 5 minutes before being added to 5 mL of AuNPs solution (30, 60 and 90 nm). EDC functioned as a linker for the conjugation of AuNPs with b-GQDs. It worked by activating the carboxyl groups on GQDs so that they could attach to amine groups of synthesized AuNPs, thus creating a strong and stable bond between AuNPs and b-GQDs. Thereafter, 1 mL of PBS (pH 7.4) was added to 4 mL of b-GQDs, and sonicated for 5 mins. Both AuNPs and b-GQDs solutions were mixed and further shaken for 1 hour using a vortex. The conjugated products were named Sample K, for b-GQDs with 30 nm AuNPs, while Sample L was with 60 nm AuNPs and Sample M for 90 nm AuNPs.

Table 2. Summary of synthesis parameters of AuNPs samples.

Sample	Sample ID	Amount of Au Seeds (mL)	Volume of gold chloride at growth stage (mL)	Hydroxylamine hydrochloride
AuNPs	**H**	10	0.25	1 mL of 0.2M
	I		1.00	
	J		3.00	

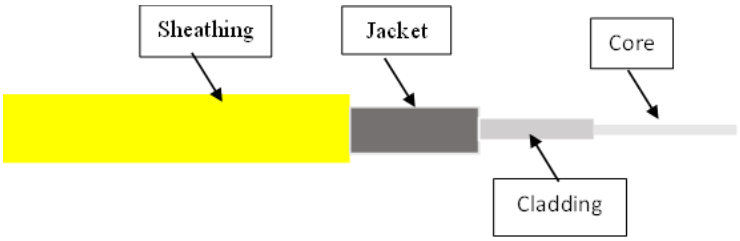

Figure 1. Layered structure of optical fibre probe.

Fabrication of a Fibre Optic Sensing Platform

Mechanical etching was used to remove the jacket and cladding layers that protected the fibre optic core. The operation started with the manual uncladding of the fibre optic protective layers with a fibre stripper. Using Figure 1 as a point of reference, beginning at the right end of the optical fibre, 8 cm of the sheathing layer was removed, then 5 cm of the jacket layer was removed, and finally, 3 cm of the cladding layer was removed. The core end of the optical fibre was subsequently cleaved with a Sumitomo FC-8R Precision Automatic Blade Rotation Fibre Cleaver. The exposed core of the optical fibre was then cleaned with an alcohol swab to remove the excess protective coating and to prevent dust from remaining on the core surface. The core region was then prepared for coating using sensing materials compounds. This was accomplished by thoroughly immersing the core region of the probe in a solution containing pure b-GQDs (Sample E), pure AuNPs (Sample H, I, J) or conjugated b-GQDs-AuNPs (Sample K, L, M) for 24 hours before drying the coated probe for another 12 hours at room temperature. The core was then spliced using a Sumitomo Type-39 Fast Cat Core Alignment Fusion Splicer Kit 1 to ensure the connection of the core with another cable probe, completing the detection circuit.

Characterization of b-GQDs, AuNPs, b-GQDS-AuNPs and the Sensing Platform

The physical observation of blue fluorescence emission of GQDs was performed using a mini portable UV lamp LED (light wavelength 365 nm). UV-Visible spectroscopy (JASCO, V-670 UV-VIS-NIR Spectrophotometer) was used to determine the optical properties of the sample. The scan range was between 200 nm and 1000 nm for AuNPs and conjugated b-GQDs-AuNPs, with all samples being 1 % v/v diluted with DI water. Each sample was measured in the absorption mode, with a quartz-type cuvette filled with water as the standard. The particle size and dispersity of the AuNPs after synthesis were characterized (Model ZEN3600) while the photoluminescence (PL) of the fluorescence signal of b-GQDs was measured using a Fluorescence Spectrophotometer F-2700. The X-ray diffraction (XRD) analysis was performed using an X-ray diffractometer (Ultima IV) with a diffraction scan range (2Θ) of 10° to 60°. The Ocean Optics spectrometer (HR400CG-UV-NIR), the SDL-1064-500M72 laser power supply, the SDL-785-LM-500M72 laser light source, and the optical fibre fusion splicer (Sumitomo Type-39, USA) were all components of the fibre optic sensor configuration.

RESULTS AND DISCUSSIONS

Characterization of b-GQDs

The formation of b-GQDs can be observed in Figure 2. Once the citric acid was heated in a microwave, the powder was observed to melt into a colourless liquid after five minutes of heating, then into a pale-yellow liquid after ten minutes, and finally into a brown-caramel viscous liquid after twenty minutes, as shown in Figure 2 (a). The addition of NaOH and HCl further diluted the colour of the solution as observed in Figures 2 (b) and (c).

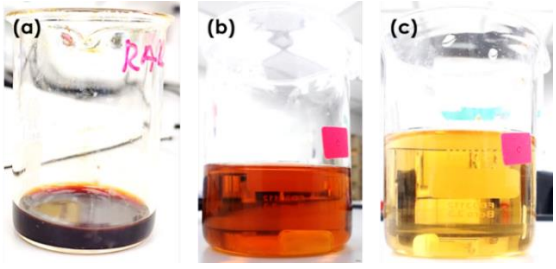

Figure 2. (a) Formation of brown-caramel solution after microwave, (b) after addition of NaOH and (c) final b-GQDs solution after pH adjustment using HCl.

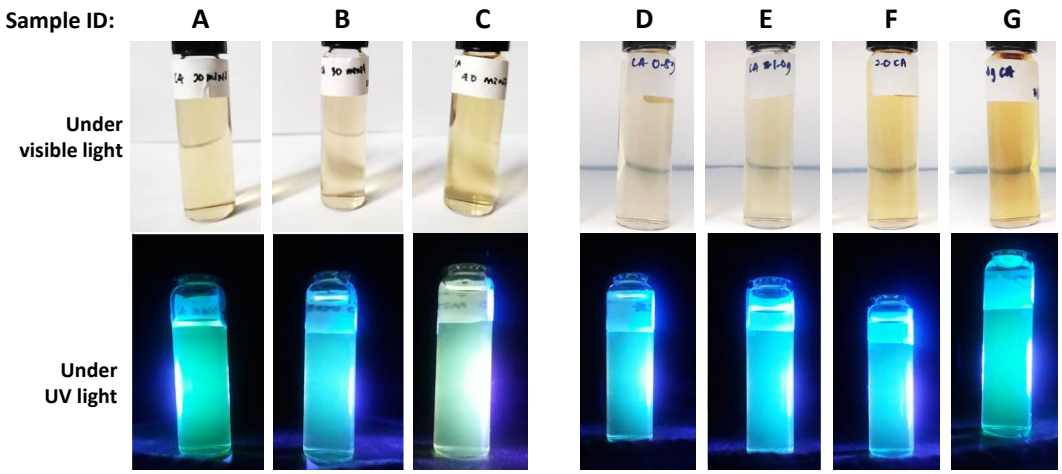

Figure 3. The synthesized b-GQDs samples with various microwave heating times (A) 20, (B) 30 and (C) 40 mins, while various weights of citric acid; (D) 0.5, (E) 1, (F) 2 and (G) 3 g at visible and UV light.

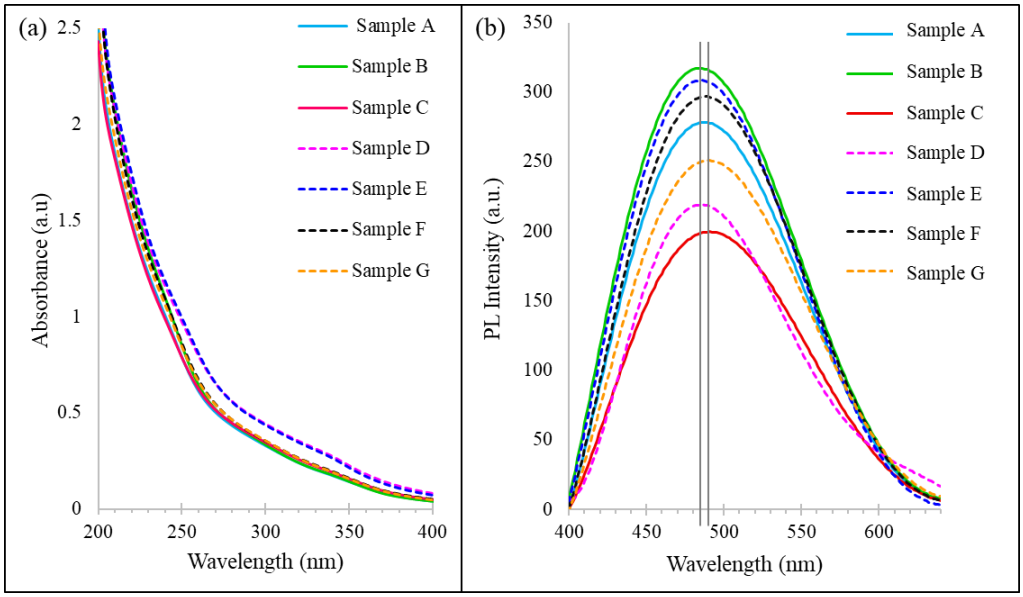

Figure 4. Measurement of b-GQDs of (a) UV-Vis spectra and (b) PL emission under excitation at 390 nm.

The first characterization of synthesized b-GQDs was conducted by exciting the b-GQDs samples with UV light (365 nm) to validate their fluorescence emission as captured in Figure 3. According to observations, 30 minutes of microwave time was found to be the optimum heating time to produce blue emission b-GQDs (Figure 3 B), when prolonged to 40 minutes, the b-GQDs started to emit a greenish colour (Figure 3 C). The intense emission of the blue fluorescence appeared at the lower weight of citric acid used (Figure 3 D-F) and became a more greenish colour when the higher weight of citric acid was used (Figure 3 G).

UV-Vis absorption and PL spectra were used to investigate the optical properties of b-GQDs samples. The colours of the substances were directly affected by absorption in the visible spectrum. As shown in Figure 4 (a), Sample E had the highest maximum absorption peak of 1.03 a.u at 248 nm compared to Sample G, which had the lowest maximum absorption peak of 0.9 a.u at 248 nm. Absorption peaks have been linked to $\pi - \pi$ and $\pi - \pi$ transitions between oxygen/nitrogen-containing groups and sp^2 domains [13], [14]. The PL wavelengths of the b-GQDs samples did not change at different wavelengths but significantly affected their emission intensity, as illustrated in Figure 4(b), showing their excitation-independent features. The difference in excitation wavelength determined the colour of the b-GQDs fluorescence. The PL peak emission of b-GQDs was observed to be around 480 to 490 nm, indicating that all samples emitted blue to greenish fluorescence

within the UV range of excitation. For strong blue-emission samples, the excitation wavelength was found at 485 nm (see Samples B, D, E and F of Figure 4, b), while a right shift to 490 nm was observed for greenish-emission samples (see Samples A, C and G of Figure 4, b), confirming the result obtained in Figure 3.

According to Liu et al. [15], in general, decreasing the size of GQDs will increase the PL intensity; meanwhile, increasing the size of GQDs will result in a red shift of the PL emission peak. As the size of the GQDs increases, their energy gap continues to decrease, and photons are more likely to transition, which results in a red shift of the PL emission peak. As observed in the fluorescence emission in Figure 3 and PL emission in Figure 4(b), the difference in colour emissions and PL intensity and peak were closely related to the surface chemistry and size of the synthesized GQDs, which were influenced by both microwave heating time and the amount of citric acid used.

20 mins of microwave heating time with 2 g of citric acid produced pale greenish-blue GQDs, indicating incomplete carbonization and the presence of many surface defects, which may have created mid-gap energy levels that resulted in a lower-energy PL peak measurement (see Sample A, Figure 3 and Figure 4, b). Meanwhile, 30 mins of microwave heating time produced smaller GQDs with more uniform size and fewer defects, resulting in strong blue fluorescence emission and higher PL energy (see Sample B, Figure 3 and Figure 4, b). However, prolonging to 40 mins of heating time allowed the GQFs to grow to a larger size, hence reducing the band gap and shifting the PL to lower energy (see Sample C, Figure 3 and Figure 4, b). A similar trend was observed when various amounts of citric acid were used with 30 mins microwave heating time. At a lower amount of citric acid (2 g and below), there was likely limited carbon available, hence producing smaller GQDs with blue emission and higher PL energy. However, using 3 g of citric acid produced a green emission, indicating that the excess carbon led to the formation of larger GQDs or more surface defects, again reducing the band gap and shifting the PL to green. Thus, the highest PL signal from the b-GQDs in Sample B (see Figure 4 (b)) indicated that 30 minutes was the optimum microwave heating time for dissolving most of the carbon into the b-GQDs structure. Furthermore, 1 g of citric acid with 30 minutes of heating time was found to be the optimum condition for synthesizing a high blue emission signal, as shown by the PL signal of Sample E in Figure 4(b).

Sample E was further analyzed by XRD spectroscopy to obtain the crystallographic information of b-GQDs. The XRD pattern in Figure 5 shows a broad plane of (002) with a diffraction peak at $2\Theta=26°$. Furthermore, the large and broad peak observed indicated that the b-GQDs prepared had extremely small particle sizes that were distinct from those of crystalline graphite (as evidenced by the acute peak at 26º). Additionally, the amorphous character of the oxygenated functional groups was observed to result in a peak broadening. By employing Bragg's law, $\lambda = 2d \sin \Theta$, where λ is the wavelength of the X-ray radiation used to irradiate the sample, d is the d-spacing between the lattice planes, and θ is the measured diffraction angle, the interlayer spacing of the b-GQDs was determined to be 3.42 Å. This value was identical to that of graphene, in agreement with [15, 16], indicating that the b-GQDs of Sample E had been successfully synthesized.

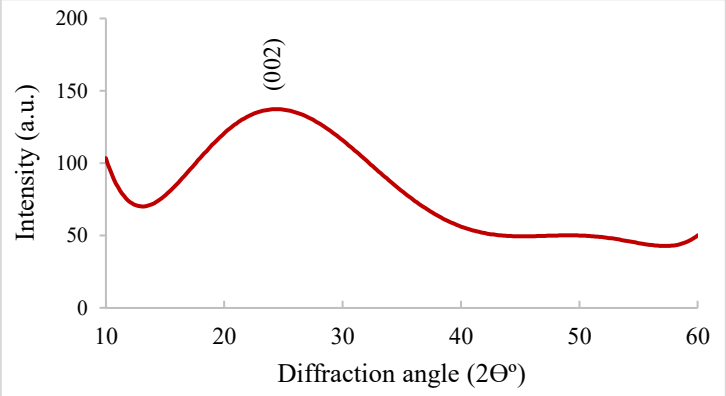

Figure 5. XRD pattern of b-GQDs of Sample E.

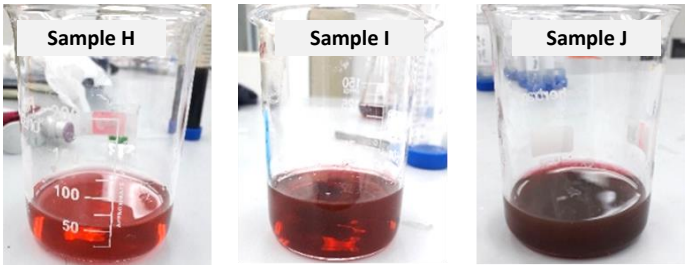

Figure 6. The different ruby red colours of synthesized AuNPs for Sample H; 30 nm, I: 60 nm and J: 90 nm obtained after adding 0.25, 1 and 3 mL of gold chloride at the growth stage.

Characterization of AuNPs

According to the physical observations shown in Figure 6, the red colour on AuNPs became more intense as the volume of gold chloride used at the growth stage increased from 0.25 mL (Sample H), 1 mL (Sample I) and further to 3 mL (Sample J). The intense colour observed in the AuNPs solutions was a result of the collective oscillation of free conduction electrons, which resonated with the frequency of incident light and produced characteristic optical absorption [17], [18]. This was supported by the optical densities obtained from the absorption intensity of the UV-Vis results, as shown in Table 3.

The summary from the UV-Vis spectrometer and zeta sizer measurement has been presented in Table 3. Sample J had the highest maximum absorption peak of 1.476 a.u at a wavelength of 528 nm, Sample I had the absorption peak at 525 nm with the intensity of 0.524 a.u, and Sample H exhibited the lowest absorption of 0.234 a.u at 522 nm. The maximum absorption peak (λ_{max}) for each sample showed a progressive red shift as the amount of gold chloride increased during the AuNPs synthesis process. The shift indicated that the size of the AuNPs increased with higher precursor volume, as supported by zeta sizer measurement. This was due to the SPR peak of AuNPs being highly size-dependent. As the particle size increased, the SPR peak shifted to longer wavelengths (a red shift) and the absorption band became broader. This occurred due to increased electron oscillation damping and enhanced scattering effects in larger particles. In contrast, smaller AuNPs exhibited blue-shifted SPR peaks (shorter wavelengths), as a result of quantum confinement and lower scattering losses [12].

The mean diameter size values of Z AuNPs increased as the amount of gold chloride used increased. The largest AuNPs, approximately 90 nm (sample J), were produced when 3 mL of gold chloride was used (with a standard deviation of 35.45 nm), supporting earlier findings in UV-Vis studies. In the Zeta sizer, the intensity of the solution was measured using dynamic light scattering (DLS), which measured the hydrodynamic diameter, i.e. the diameter of the particles with an extra layer of solvent around it in the dispersed phase [17]. A smaller PDI value closer to 0 for all three samples indicated that the nanoparticles were well distributed in suspension (close to monodisperse) and not aggregates/agglomerates. The synthesis of AuNPs (sample H) with an average size of 30 nm was successful due to the use of a smaller amount of gold chloride with a lower standard deviation as compared to sample I.

Characterization of Conjugated b-GQDs-AuNPs

UV–Vis absorption spectroscopy was used to investigate the optical properties of hybrid nanomaterials. The b-GQDs-AuNPs samples demonstrated a peak at around 238 nm, which corresponded to the n-π* transitions of C-O bonds speculated due to the absorption of the graphitic structure as shown in Figure 7.

Table 3. Summary of UV-Vis absorption spectra and Zeta sizer measurement of synthesized AuNPs.

AuNPs Sample ID	UV-Vis measurement		Zeta sizer measurement		
	λ_{max} (nm)	Absorbance Intensity (Optical density, OD)	Particle Size (nm)	Stand. dev (nm)	PDI
H	522	0.2345	50.73	20.26	0.299
I	525	0.5248	58.60	25.91	0.285
J	527	1.4760	68.76	35.45	0.442

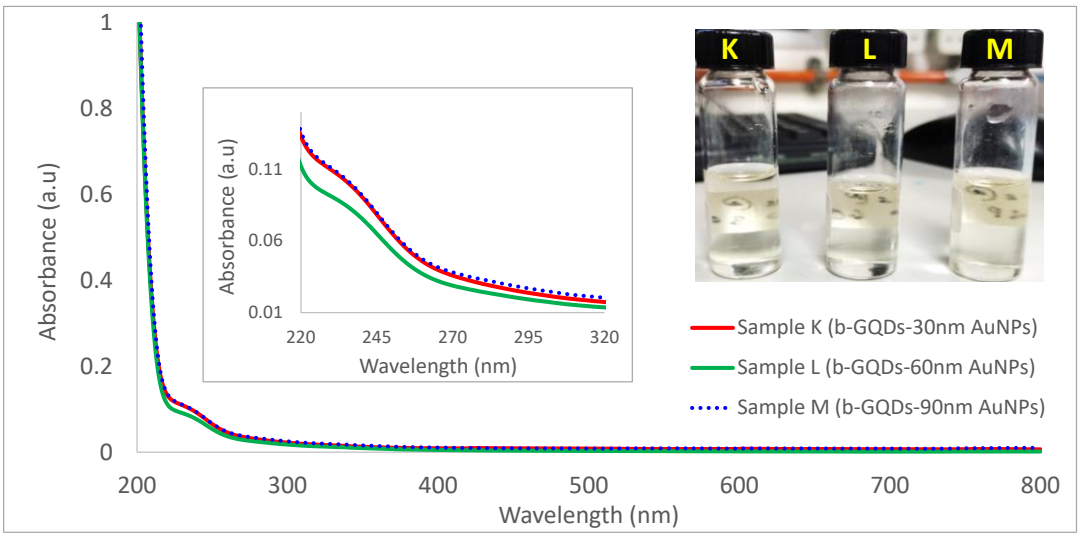

Figure 7. UV-Vis absorption spectra of conjugated b-GQDs with 30, 60 and 90 nm AuNPs. The magnified figure shows the interest peak absorption area. Inset: Photograph taken of samples under visible light.

Signal Testing on Optical Fibre Coated with GQDs, AuNPs and Conjugated b-GQDs-AuNPs

In general, the sensing mechanism of the modified fibre optic sensors is based on the optical intensity changes resulting from the interaction of the evanescent field of the propagation light with the sensing materials deposited on the surface of the structure [19]. Once any molecules are entrapped at the surface of the deposited materials, the optical properties will be modulated accordingly, as measured by the spectrometer. Figure 8 shows the signal detected from the spectroscopy when each of the different coating nanomaterials was used to coat the modified SOF probe. The signal was significantly amplified when the probe was coated with the nanomaterials, when compared to the bare/uncoated probe. The result is in agreement with [20]. Compared to the uncoated probe, the signal generated by AuNPs-coated probes gradually increased as the AuNPs got smaller, with 30 nm AuNPs (Sample H) having the highest output compared to other AuNPs samples. Meanwhile, pure b-GQDs (Sample E) coated probe significantly improved the signal to 84.9%. Interestingly, the sensor signal generated from the sensing platform of hybrid b-GQDs-30nm AuNPs (Sample K) coated probe showed the highest signal, surpassing the other samples with a 143.5% increment from the uncoated probe, as shown in Table 4.

Table 4. Summary of the signal of the sensor measured from various coating materials extracted from Figure 10.

Sample ID	Coating material	Signal reading		Signal Improvement, % (vs. uncoated probe)
		Light intensity (count)	Stdv. dev (count)	
E	b-GQDs	2822.12	176.64	84.9
H	30 nm AuNPs	2175.22	88.68	42.5
I	60 nm AuNPs	2057.62	93.41	34.8
J	90 nm AuNPs	1913.79	75.37	25.4
K	**GQDs-30nm AuNPs**	**3715.97**	**271.85**	**143.5**
L	GQDs-60nm AuNPs	3245.09	173.35	112.6
M	GQDs-90nm AuNPs	2270.43	97.27	48.8
Control	Uncoated (bare probe)	1526.18	40.63	0.0

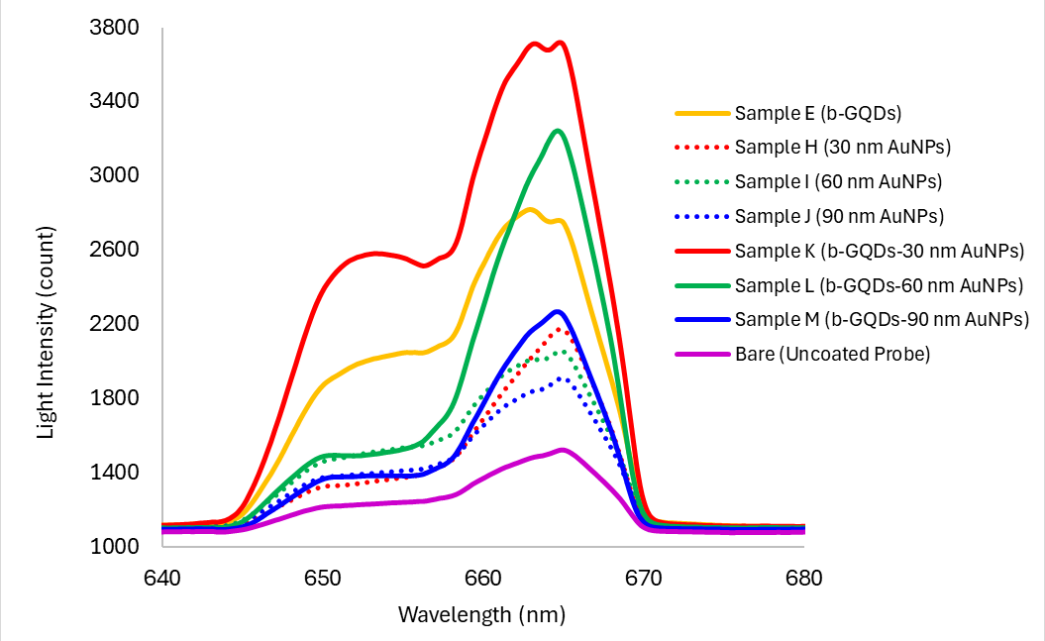

Figure 8. Signal detection using a fibre optic sensor with various coating materials on the sensing platform of the fibre optic probe.

This evidence shows that the sensor signal can be significantly amplified when the hybrid structure is used with a smaller size of AuNPs and works better with b-GQDs. The results also proved that smaller nanoparticles provide a higher detection signal, as with a decrease in size, the surface area increases, and the nanostructure will have more surface area for the reaction. Hence, reactivity increases with a decrease in particle size. This outcome demonstrated that hybrid nanoparticles of b-GQDs with 30 nm AuNPs (Sample K) provide excellent load transfer capacity, making them ideal for lower detection limits and higher sensitivity values, which are valuable properties for various advanced sensor applications, including biosensors.

CONCLUSIONS

A series of greenish to blue fluorescence emissions of b-GQDs was successfully synthesized using microwave-assisting method using citric acid as a carbon precursor. The optimum b-GQDs sample with strong blue fluorescence emission, with a d-spacing of 3.42 Å, was formed from 2 g of citric acid with 30 minutes of microwave heating time. The synthesized sizes of 30, 60 and 90 nm of AuNPs was confirmed via UV-Vis wavelength spectra and particle size analysis. The performance of the optical fibre sensor with sensing material of a hybrid with b-GQDs-30nm AuNPs samples demonstrated superior signal detection with the generation of up to 84.9% of pure b-GQDs coating samples and 42.5% of 30 nm AuNPs samples. In addition, the smaller size of nanoparticles as sensing materials provided greater signals than the larger size. The study had shown a significant outcome, that this newly integrated hybrid nanostructure of b-GQDs conjugated 30 nm AuNPs provides superior sensing behaviour as the signal was boosted to 143.5 % compared to the uncoated probe, which shows promise for further exploration in constructing rapid, robust, and highly sensitive fibre optic sensors.

ACKNOWLEDGEMENT

The authors would like to acknowledge the funding from AEH Innovative Hydrogel Ltd, UK, for the international industry grant (100-TNCPI/INT 16/6/2 (007/2020)). The authors significantly valued the technical support from the Faculty of Mechanical Engineering, Photonics Research Centre, IoS UiTM and NANO-Electronic Research Group, Universiti Teknologi MARA (UiTM), Shah Alam, Selangor, Malaysia.

The authors declare that they have no conflict of interest.

REFERENCES

1. Wang, X. D. & Wolfbeis, O. S. (2016) Fiber-optic chemical sensors and biosensors (2013–2015). *Analytical chemistry*, **88(1)**, 203–227.

2. Dissanayake, K. P. W., Wu, W., Nguyen, H., Sun, T. & Grattan, K. T. (2017) Graphene-oxide-coated long-period grating-based fiber optic sensor for relative humidity and external refractive

index. *Journal of Lightwave Technology*, **36(4)**, 1145–1151.

3. Zhao, Y., Li, X. G., Zhou, X. & Zhang, Y. N. (2016) Review on the graphene based optical fiber chemical and biological sensors. *Sensors and Actuators B: Chemical*, **231**, 324–340.

4. Facure, M. H., Schneider, R., Lima, J. B., Mercante, L. A. & Correa, D. S. (2021) Graphene quantum dots-based nanocomposites applied in electrochemical sensors: A recent survey. *Electrochem*, **2(3)**, 490–519.

5. Lah, C. N. H. C., Jamaludin, N., Rokhani, F. Z., Rashid, S. A. & Noor, A. S. M. (2019) Lard detection using a tapered optical fiber sensor integrated with gold-graphene quantum dots. *Sensing and Bio-Sensing Research*, **26**, 100306.

6. Hossain, N., Rimon, M. I. H., Mimona, M. A., Mobarak, M. H., Ghosh, J., Islam, M. A. & Al Mahmud, M. Z. (2024) Prospects and challenges of sensor materials: A comprehensive review. *e-Prime-Advances in Electrical Engineering, Electronics and Energy*, **7**, 100496.

7. Animashaun, C., Lahcen, A. A. & Slaughter, G. (2025) Gold Nanoparticle-Enhanced Molecularly Imprinted Polymer Electrode for Non-Enzymatic Lactate Sensing. *Biosensors*, **15(6)**, 384.

8. Ganesh, K. M., Bhaskar, S., Cheerala, V. S. K., Battampara, P., Reddy, R., Neelakantan, S. C., Reddy, N. and Ramamurthy, S. S. (2024) Review of gold nanoparticles in surface plasmon-coupled emission technology: Effect of shape, hollow nanostructures, nano-assembly, metal–dielectric and heterometallic nanohybrids. *Nanomaterials*, **14(1)**, 111.

9. Fakhri, M. A., Salim, E. T., Tariq, S. M., Ibrahim, R. K., Alsultany, F. H., Alwahib, A. A., Alhasan, S. F. H., Gopinath, S. C., Salim, Z. T. and Hashim, U. (2023) A gold nanoparticles coated unclad single mode fiber-optic sensor based on localized surface plasmon resonance. *Scientific Reports*, **13(1)**, 5680.

10. Makhsin, S. R., Zakaria, M. H., Akashah, M. H. N., Rani, R. A., Scully, P. J. & Gardner, P. (2023) Enhancing fibre optic sensor signals via gold nanoparticle-decorated agarose hydrogels. *Optical Materials*, **143**, 114247.

11. Van Tam, T., Hur, S. H., Chung, J. S. & Choi, W. M. (2021) Novel paper-and fiber optic-based fluorescent sensor for glucose detection using aniline-functionalized graphene quantum dots. *Sensors and Actuators B: Chemical*, **329**, 129250.

12. Rabizah Makhsin, S., Razak, K. A., Noordin, R., Dyana Zakaria, N. & Chun, T. S. (2012) The effects of size and synthesis methods of gold nanoparticle-conjugated MαHIgG 4 for use in an immunochromatographic strip test to detect brugian filariasis. *Nanotechnology*, **23(49)**, 495719.

13. Ting, S. L., Ee, S. J., Ananthanarayanan, A., Leong, K. C. & Chen, P. (2015) Graphene quantum dots functionalized gold nanoparticles for sensitive electrochemical detection of heavy metal ions. *Electrochimica Acta*, **172**, 7–11.

14. Yoon, H., Chang, Y. H., Song, S. H., Lee, E. S., Jin, S. H., Park, C., Lee, J., Kim, B. H., Kang, H. J., Kim, Y. H. and Jeon, S. (2016) Intrinsic Photoluminescence Emission from Subdomained Graphene Quantum Dots. *Advanced Materials (Deerfield Beach, Fla.)*, **28(26)**, 5255–5261.

15. Liu, Z., Li, F., Luo, Y., Li, M., Hu, G., Pu, X., Tang, T., Wen, J., Li, X. and Li, W. (2021) Size effect of graphene quantum dots on photoluminescence. *Molecules*, **26(13)**, 3922.

16. Ziegler, C. & Eychmuller, A. (2011) Seeded growth synthesis of uniform gold nanoparticles with diameters of 15− 300 nm. *The Journal of Physical Chemistry C*, **115(11)**, 4502–4506.

17. Saha, K., Agasti, S. S., Kim, C., Li, X. & Rotello, V. M. (2012) Gold nanoparticles in chemical and biological sensing. *Chemical Reviews*, **112(5)**, 2739–2779.

18. Shehab, M., Ebrahim, S. & Soliman, M. (2017) Graphene quantum dots prepared from glucose as optical sensor for glucose. *Journal of Luminescence*, **184**, 110-116.

19. Dong, Y., Shao, J., Chen, C., Li, H., Wang, R., Chi, Y., Lin, X. and Chen, G. (2012) Blue luminescent graphene quantum dots and graphene oxide prepared by tuning the carbonization degree of citric acid. *Carbon*, **50(12)**, 4738–4743.

20. Roslan, A. H., Makhsin, S. R., Abdul Rani, R. & Siddique, B. (2024) Amplifying fibre optic sensor signals with graphene oxide-silver nanostars. *Journal of Mechanical Engineering (JMechE)*, **21(3)**, 297–317.